Spectroscopy Letters, 38: 343–363, 2005

ISSN 0038-7010 print/1532-2289 online
DOI: 10.1081/SL-200058715

Application of Synchrotron X-Ray Microbeam Spectroscopy to the Determination of Metal Distribution and Speciation in Biological Tissues

T. Punshon
Consortium for Risk Evaluation with Stakeholder Participation, Environmental and Occupation Health Sciences Institute, Division of Life Sciences, Rutgers University, Piscataway, New Jersy, USA

B. P. Jackson
Savannah River Ecology Laboratory, University of Georgia, Aiken, South Carolina, USA

A. Lanzirotti
Consortium for Advanced Radiation Sources, The University of Chicago, Chicago, Illinois, USA

W. A. Hopkins and P. M. Bertsch
Savannah River Ecology Laboratory, University of Georgia, Aiken, South Carolina, USA

J. Burger
Consortium for Risk Evaluation with Stakeholder Participation, Environmental and Occupation Health Sciences Institute, Division of Life Sciences, Rutgers University, Piscataway, New Jersy, USA

Received 12 June 2004, Accepted 22 October 2004

This paper was by special invitation as a contribution to a special issue of the journal entitled "Application of Spectroscopic Methods to Environmental Problems." The special issue was organized by Professor Peter A. Tanner, Professor in the Department of Biology and Chemistry at City University of Hong Kong.

Address correspondence to T. Punshon, Consortium for Risk Evaluation with Stakeholder Participation, Environmental and Occupation Health Sciences Institute, Division of Life Sciences, Rutgers University, 604 Allison Road, Piscataway, NJ 08854, USA. E-mail: punshon@srel.edu

Abstract: Resolving the distribution and speciation of metal(loid)s within biological environmental samples is essential for understanding bioavailability, trophic transfer, and environmental risk. We used synchrotron x-ray microspectroscopy to analyze a range of samples that had been exposed to metal(loid) contamination. Microprobe x-ray fluorescence elemental mapping (μSXRF) of decomposing rhizosphere microcosms consisting of Ni- and U-contaminated soil planted with wheat (*Triticum aestivum*) showed the change in Ni and U distribution over a 27-day period, with a progressive movement of U into decaying tissue. μSXRF maps showed the micrometer-scale distribution of Ca, Mn, Fe, Ni, and U in roots of willow (*Salix nigra* L.) growing on a former radiological settling pond, with U located outside of the epidermis and Ni inside the cortex. X-ray computed tomography (CMT) of woody tissue of this same affected willow showed that small points of high Ni fluorescence observed previously are actually a Ni-rich substance contained within an individual xylem vessel. μSXRF and x-ray absorption near-edge spectroscopy (XANES) linked the elevated Se concentrations in sediments of a coal fly ash settling pond with oral deformities of bullfrog tadpoles (*Rana catesbeiana*). Se distribution was localized within the deformed mouthparts, and with an oxidation state of Se (− II) consistent with organo-Se compounds, it suggests oral deformities are caused by incorporation of Se into proteins. The range of tissues analyzed in this study highlight the applicability of synchrotron X-ray microspectroscopic techniques to biological tissues and the study of metal(loid) bioavailability.

Keywords: Biological tissue, micro-XANES, nickel, selenium, synchrotron x-ray fluorescence, uranium, x-ray fluorescence microtomography

INTRODUCTION

The use of a synchrotron x-ray fluorescence microprobe (μSXRF) to determine the distribution of metals and metalloids in heterogeneous biological samples is rapidly growing.[1–3] The excellent detection sensitivity of μSXRF (with limits in the sub $\mu g\, g^{-1}$ range) enables rapid elemental mapping of a variety of materials. Coupled with the smaller source size of second- and third-generation synchrotron facilities that produce focused, hard x-ray microbeams $<1\,\mu m$ in diameter, spatial metal analysis on a $0.5-1\,\mu m$ scale is now feasible. Elemental maps can be used to identify cells, tissues, or inclusions that have distinct metal concentrations in biological samples. Distribution characteristics such as elemental co-association can provide information about modes of action, transport, or toxicity. Once areas of elevated metal abundance are identified, x-ray absorption spectroscopy (XAS), comprising x-ray absorption near-edge spectroscopy (XANES) and extended x-ray absorption fine structure spectroscopy (EXAFS), can evaluate the oxidation state of the metal, and under certain conditions, the number, identity and distance ($\pm$ 0.02 Å) of its neighboring atoms. Increasingly, the use of an x-ray microprobe is being used to answer quantitative as well

as qualitative questions about metal bioavailability with minimal sample alteration.[4,5]

There are numerous examples of the application of x-ray spectroscopic techniques to biological tissue, with a preponderance of studies in the clinical and environmental sciences. In the former instance, synchrotron radiation has been used to analyze the distribution and quantification of Zn and Ca in cancerous prostate tissues,[6] eliminating the isolation and purification stages, and finding a role for Ca in the control of Zn transport into prostate tissues. The distribution and chemical form of Fe in brain tissue from patients who died of Parkinson disease was investigated using similar techniques.[7] Szczerbowska-Boruchgowska et al.[8] also used μSXRF to examine cellular mechanisms of Parkinson's disease, finding Fe accumulation in structures that had not been previously identified histopathologically, emphasizing the micrometer-scale precision in samples too fragile for conventional dissection. In this case, the technique was able to compare the elemental concentration ($\mu g\,cm^{-1}$) of individual neurons in healthy and diseased tissues.

In a similar manner to the mechanistic applications of the clinical sciences, μSXRF can be used to determine the effects of inorganic contaminants on biota. The majority of studies have been carried out on plant material, and comparatively little on invertebrates, amphibians, fish, and other affected wildlife. This may be due to the very low metal concentrations typical of higher trophic level terrestrial biota and the ease by which plant samples can be sampled and prepared for analysis. For plants, researchers are elucidating mechanisms of metal uptake, toxicity, and tolerance. An understanding of the metal metabolism of hyperaccumulating plants is necessary for the development of plant-based soil remediation technologies (for a review, see Salt et al.[9]), and x-ray spectroscopic techniques (including particle-induced x-ray emission) are directly involved in advancing knowledge in this area. XAS has been extensively applied to hyperaccumulator plants to determine the ligands to which metals are bound.[10–15] Studies on the metal metabolism of non-hyperaccumulator plants are less common, although key studies exist.[4] This information is important for assessing potential biomagnification risk and routes in contaminated ecosystems. Overall, μSXRF studies range from the elemental distributions in the annual rings of metal-affected trees,[16–19] fossilized wood,[20,21] pine needles,[22] leaf tissue,[23,24] root tissue,[25,26] moss,[27] to that of bacteria[28] and plankton.[29]

The current study provides examples of the application of μSXRF to biota that have been exposed to metals and metalloids and have been collected either from the field or have been exposed to field-collected soils in the laboratory. These studies reflect the scope of biological samples that are amenable to SXRF and XAS analysis, including both terrestrial and aquatic biota. The sites from which samples were collected are highly representative of metal-contaminated waste sites; including an area downstream

from a former radiological settling basin and a wetland arising from a fly ash settling lagoon. Studying the ecosystems that have developed upon these waste sites allows more realistic inferences to be made about metal uptake, transport, and toxicity and provides information about potential environmental risk.[30]

MATERIALS AND METHODS

Study Sites

The Savannah River Site (SRS) is a 800 km^2 U.S. Department of Energy facility responsible for the production of nuclear weapons materials from the 1950s to the early 1990s. Currently, the core mission of the SRS is nuclear materials processing and environmental remediation. Metal and metalloid impacted biota were collected from two contaminated ecosystems on the SRS. The first is a former radiological settling pond, on which a diverse seasonal wetland ecosystem now thrives, and the second is a fly ash disposal lagoon, which receives coal combustion wastes enriched with metalloids such as Se.

Steed Pond–Lower Tims Branch Riparian Corridor

Steed Pond is one of the most important former waste units within the custodianship of the DOE,[31] having received more than 44,000 kg of depleted and natural U, similar quantities of Ni, and lesser amounts of Cu, Pb, Zn, and Cr between 1954 and 1978.[32] The pond serves as a *de facto* settling basin, receiving high volumes of metallurgical waste from a former U target fabrication facility, which was part of the plutonium production infrastructure at the SRS. As a result, the pond was unlined and separated from the riparian corridor to the south by the original wooden spillway. In the fall of 1984, the wooden spillway breached, draining the pond, releasing contaminated sediments downstream to lower Tims Branch and exposing the remaining sediments to periodic erosion. These studies build on a body of work on the geochemistry and bioavailability of contaminants in both Steed Pond and Lower Tims Branch.[19,33–39]

D-Area Ash Basins

The D-area ash basins were constructed in the late 1970s to receive waste material from an on-site coal-burning electrical power plant and are still in operation. Sluiced coal ash is pumped from the power station through a series of progressively smaller settling basins (15, 6, and 2 ha) before entering a tributary to the Savannah River. The ash suspended in the

water settles as it moves through the impoundments, resulting in highly elevated sediment concentrations of As, Cd, Cr, Cu, and Se in the pond sediments.[40] The concentrations of metals and metalloids within the ash basin sediments are (mean $\mu g\, g^{-1}$ d.wt $\pm$ standard deviation): 39.6 ($\pm$2.8) As, 0.25 ($\pm$0.01) Cd, 10.9 ($\pm$0.81) Cr, 18.4 ($\pm$1.3) Cu, and 4.3 ($\pm$0.1) Se. For the metalloids, the sediment As concentration is 116 $\times$ background (compared to a nearby reference site), and Se is 41 $\times$ background.[41]

Biota inhabiting the settling basins have elevated Se concentrations in their tissues.[42,43] Studies on the developmental and reproductive physiologies of biota in the ash basin ecosystem found abnormalities, which may reduce individual fitness.[44,45] The issue for this site therefore involves linking the high concentrations of metalloid contaminants to the observed developmental abnormalities of the amphibians using the area. An extensive review of the toxicological studies conducted on the aquatic biota in the D-area ash basins is included in Rowe et al.[41]

Study 1. Metal Distribution at the Root–Soil Interface

Roots Collected from Steed Pond

Roots were collected from an 8-year-old black willow (*Salix nigra* L.) growing on the Steed Pond former floodplain area. Air-dried root samples were embedded in a trace-metal-free liquid epoxy resin (3M Scotchcast electrical resin, Austin, TX, USA), sliced to a thickness of 30 μm with an alpha alumina wafering saw (Buehler, Lake Bluff, IL, USA) and polished with diamond paste to remove any extraneous metals deposited on the surface during slicing. Samples were mounted on a trace-metal-free silica glass slide. Sample preparation was conducted by Spectrum Petrographics (Winston, OR, USA).

Synchrotron x-ray microprobe analyses were conducted at beamline X26A of the National Synchrotron Light Source (Brookhaven National Laboratory, Upton, NY, USA). For compositional mapping, the incident X-ray beam was tuned to 17.5 keV using a Si(111) channel-cut monochromator. The beam was focused using rhodium-coated Kirkpatrick–Baez focusing optics.[46] A beam size of 5 $\times$ 10 μm (x axis and y axis, respectively) was used for the whole-root sections, with a step size of 75 μm and a dwell time of 2 s pixel^{-1}. For root cross-sections, a 10 $\times$ 15 μm beam area was used, with a 30-μm step size and a 5-s pixel^{-1} dwell time. Step size distribution was determined primarily by considering the overall sample heterogeneity and size; for instance, where the individual cell sizes are small, smaller step sizes were used. In general, to gain as detailed a resolution as possible, smaller step sizes (no more than 10 times the size of the beam dimensions in either the x or y axes) were used. It should be noted that determination

of step sizes also took time constraints into consideration. Dwell times per pixel were optimized by collecting XRF spectra from the sample, and determining the minimum time required for adequate peak resolution. Energy dispersive x-ray fluorescence data were collected using a Canberra SL30165 Si(Li) detector (Meriden, CT, USA). Detection limits for the majority of elements are between $0.1-10\,\mathrm{mg\,kg^{-1}}$.

Uranium and Nickel in Micro-Rhizospheres

Elemental maps of Steed Pond soil suggested that U preferentially binds to organic features,[34] such as decaying plant roots or invertebrates. The aim of this study was to investigate the differential partitioning of Ni and U within decaying root material in the soil profile.

Contaminated soils were collected from the depositional environment at Lower Tims Branch. Uranium and Ni concentrations were 804 and $265\,\mu\mathrm{g\,g^{-1}}$ d.wt, respectively. Soil was dried (105°C for 48 hr), sieved (2 mm), and homogenized. The microcosm setup consisted of 21×50 mL free-draining terracotta plant pots, containing two stacked resin-embedding rings (2 cm diameter × 2 cm height) (Buehler, Lake Bluff, IL, USA) taped together on the outside. The pots and rings were filled with soil and wheat seeds (*Triticum aestivum* L.) were planted within the rings at a rate of 3 seeds per pot. Plants were maintained in an environmental growth chamber (25 ± 1°C, 16:8 hr light:dark cycles) with daily watering until substantial root growth could be seen emerging from the bottom of the pots; approximately 14–16 days. Plants were killed by excising the leaves at the junction with the seed. Three micro-rhizospheres were prepared for μSXRF analysis 5 days and 32 days after the plants were killed.

Embedding rings were removed from pots and placed in rubber embedding cups while still moist, taking care not to dislodge the soil from the root mat. The samples were dried at 60°C for 48 hr. Trace metal free electrical epoxy resin (3M Scotchcast) was poured directly into the rings and cured at 70°C for 2 days. Embedded micro-rhizospheres were sliced with a diamond wafering saw to 1-mm thick.

μSXRF analyses were conducted at beamline X26A of the National Synchrotron Light Source using a Si(111) channel cut monochromator as described above. Fluorescence counts from micro-rhizosphere analyses were collected using a Canberra 9-element Ge Array detector. Incident beam intensity was monitored using an ion chamber, and monochromator energy was 11.8 keV for Ca, Fe, Ni, and Cu analysis and 17.2 keV for U analysis. The incident beam area was $5\,\mu\mathrm{m} \times 6\,\mu\mathrm{m}$; 5-day-old samples were mapped using a step size of 30 μm (*x* axis) and 50 μm (*y* axis) with a dwell time of $3\,\mathrm{s\ pixel^{-1}}$, whereas 32-day-old samples were mapped with a 20 μm (*x* axis) and 60 μm (*y* axis) step and a $3\,\mathrm{s\ pixel^{-1}}$. For the current qualitative studies, ion chamber normalized fluorescence counts were used as indications

of metal distribution, however, methodology for the quantification of normalized fluorescence data is described in full in Punshon et al.[19]

Study 2. X-Ray Fluorescence Computed Microtomography of Ni in the Vascular System of *Salix nigra* L.

Previous observations of the distribution of Ni within the woody tissue of black willows (*Salix nigra* L.) inhabiting Steed Pond have revealed small, localized areas of elevated Ni contrasting with a diffuse distribution within woody tissue.[19] Comparisons with elemental maps of structural elements suggested that the localized area was an almost exclusively Ni-containing substance within the lumen of a xylem vessel. To investigate this further, the area of interest was excavated from the wood tissue sample using a Merchantek micromill system (Newave, Freemont, CA, USA) fitted with a tungsten carbide round-head drill bit (Brasseler, Savannah, GA, USA). The presence of Ni was confirmed with μSXRF mapping, and the sample was mounted on a glass filament for fluorescence CMT analysis. During CMT analysis, the conventional microprobe apparatus is used with a stage that rotates about the vertical axis, known as a goniometer. The sample is mounted on the goniometer and is translated perpendicular to the beam through either 180° or 360° of rotation to yield a sinogram. For this analysis, a beam area of 15 μm (x axis) × 10 μm (y axis) was used, with 12-μm horizontal and vertical translation through 180° rotation (in 4° steps). Beamline configuration was identical to that of the steed pond roots study above, with a beam energy of 17.5 keV, a Si(111) channel-cut monochromator, and Kirkpatrick–Baez focusing optics. A Canberra SL30165 Si(Li) detector was used to collect energy dispersive x-ray fluorescence data. Reconstructions were carried out with filtered back projection using the IDL Riemann function.[47] A very basic correction was made for self-absorption effects by estimating an average absorption coefficient for the sample of wood assuming an average density of 0.42 g cm^{-3}. The fluorescence intensity was then normalized by the negative exponential of the coefficient as a function of distance from the fluorescence detector. Because of the low density of this sample, the corrections proved negligible.

Study 3. Selenium Distribution and Speciation in Deformed Mouthparts of Bullfrog Tadpoles (*Rana catesbeiana*)

Selenium is essential at low concentrations but toxic to plants and animals at higher concentrations.[48] Selenium is required for the formation of the amino acid Se-cysteine; the active site in a number of enzymes such as glutathione peroxidase. At higher concentrations, Se causes reproductive failure due to its propensity to be maternally transferred and its high embryotoxicity. Chronic Se poisoning occurs in organisms inhabiting wetlands contaminated

with coal combustion waste,[49,50] manifesting itself in various physiological abnormalities, and similar effects from chronic metal exposure are suspected at the D-area ash basins on the SRS.[40,45] This study used μSXRF and XANES analysis of organisms collected from the D-area fly ash basins to elucidate Se distribution and coordination environments.[1]

Bullfrog larvae (*Rana catesbeiana*) samples were collected from the D-area fly ash settling basin. Previous studies had shown a higher incidence of oral abnormalities compared to animals collected from a nearby reference site.[42] Furthermore, relatively high concentrations of Se ($\geq 30\,\mu g\,g^{-1}$) had previously been determined in whole larvae.[40,45] Mouthparts were sectioned and frozen ($-20^{\circ}C$), along with the remainder of the animal, prior to analysis at the Advanced Photon Source (APS), Argonne National Laboratory (Chicago, IL, USA).

SXRF mapping and μ-XANES was conducted using the x-ray microprobe at GeoSoilEnviroCARS at APS (Sector 13D, undulator line). Cryogenically cooled Si(111) monochromators and a Kirpatrick–Baez mirror systems were used to produce a beam size approximately 5 μm in diameter. μSXRF mapping was conducted at 12.721 keV, with a step size of 20 μm in both the *x* and *y* dimensions and a dwell time of $3\,s\,pixel^{-1}$. μXANES analysis in areas of elevated Se was performed over the energy range of 12.533–12.786 keV with a pre-edge step size of 10 eV, edge and near-edge step sizes of 0.5 eV, and a post-edge step size of 5 eV. Dwell times during μXANES was $5\,s\,pixel^{-1}$. For both μSXRF and μXANES analysis, detection was in fluorescence mode using a Ge 16 element detector. Selenium oxidation state standards for μXANES (sodium selenite, sodium selenate, seleno-methionine, and seleno-cystine) were prepared as solids from analytical grade standards (Sigma, St. Louis, MO, USA). A small quantity of ground solid was loaded onto Kapton metal-free adhesive tape, placed in a 35-mm slide mount prior to analysis.

RESULTS AND DISCUSSION

Study 1. Roots in Contaminated Steed Pond–Tims Branch Soils

Roots Collected from the Steed Pond Former Floodplain Area

Elemental maps generated from lignified tree roots (≈5-mm diameter) collected from a U-enriched area of Steed Pond[34] show Ca (Fig. 1a), Mn (Fig. 1b), Fe (Fig. 1c), and Ni (Fig. 1d). The distribution of Ca correlates with photomicrograph images and indicates the anatomical structure. Higher Ca concentrations were found in the cortex and cell walls of the vascular system, where it is strongly attracted to the negatively charged carboxyl groups that typically line xylem tissues. Iron and Mn were present in Steed Pond soils at elevated concentrations,[39] and this enrichment is evident in

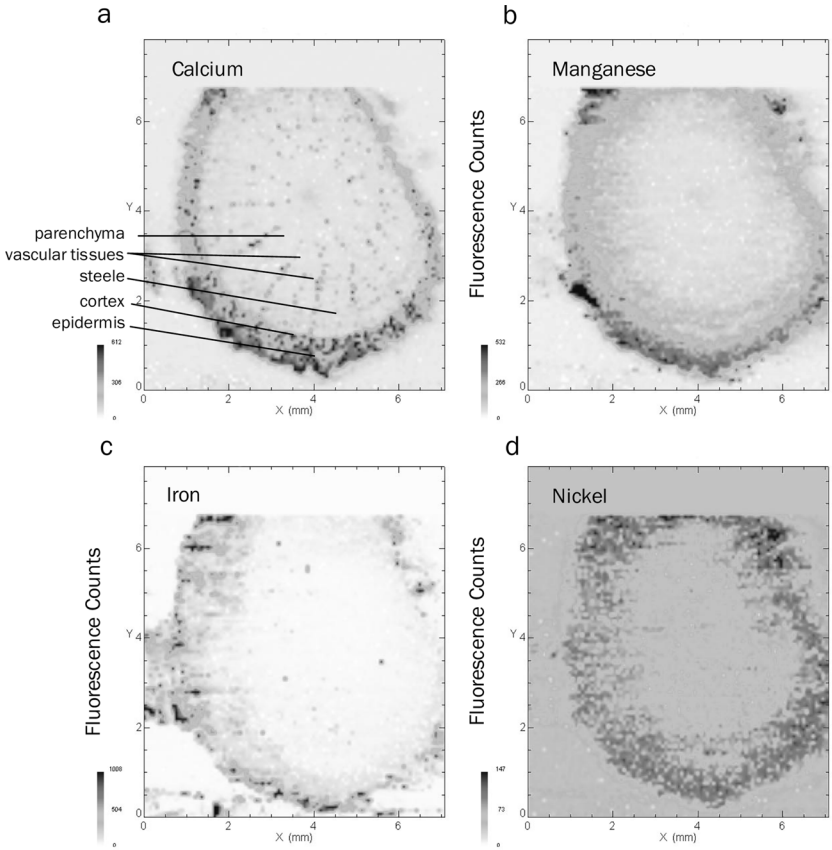

Figure 1. Micro-XRF images of sections (8 mm × 7 mm) of a woody root tissue of *Salix nigra* L. collected from a Ni- and U-contaminated wetland, showing (a) Ca, (b) Mn, (c) Fe, and (d) Ni. Legends indicate raw fluorescence counts.

elemental maps. Iron was distributed primarily in the outermost cortical regions (Fig. 1c), with higher florescence counts in the epidermis; whereas Mn was evenly distributed in the parenchymatous tissue within the steele (Fig. 1b). Similarly, Ni was found evenly distributed throughout the parenchymatous tissue of the steele and the cortex (Fig. 1d). Analysis of roots by ICP-OES indicated that they contained 156 ($\pm$7.6) $\mu g\, g^{-1}$ Ni and 139 ($\pm$ 4.2) $\mu g\, g^{-1}$ U,[51] although no U was detected in the internal tissues of the larger root cross-sections. Smaller roots were analyzed using a different experimental resolution in an attempt to detect U. A section of root from the steele to epidermis was imaged using a longer dwell time (95 s) (Fig. 2a). Elemental maps indicate that both Ni (Fig. 2b) and U (Fig. 2c) are located primarily on the outside of the root epidermis, with comparatively more Ni within the root cortex than U.

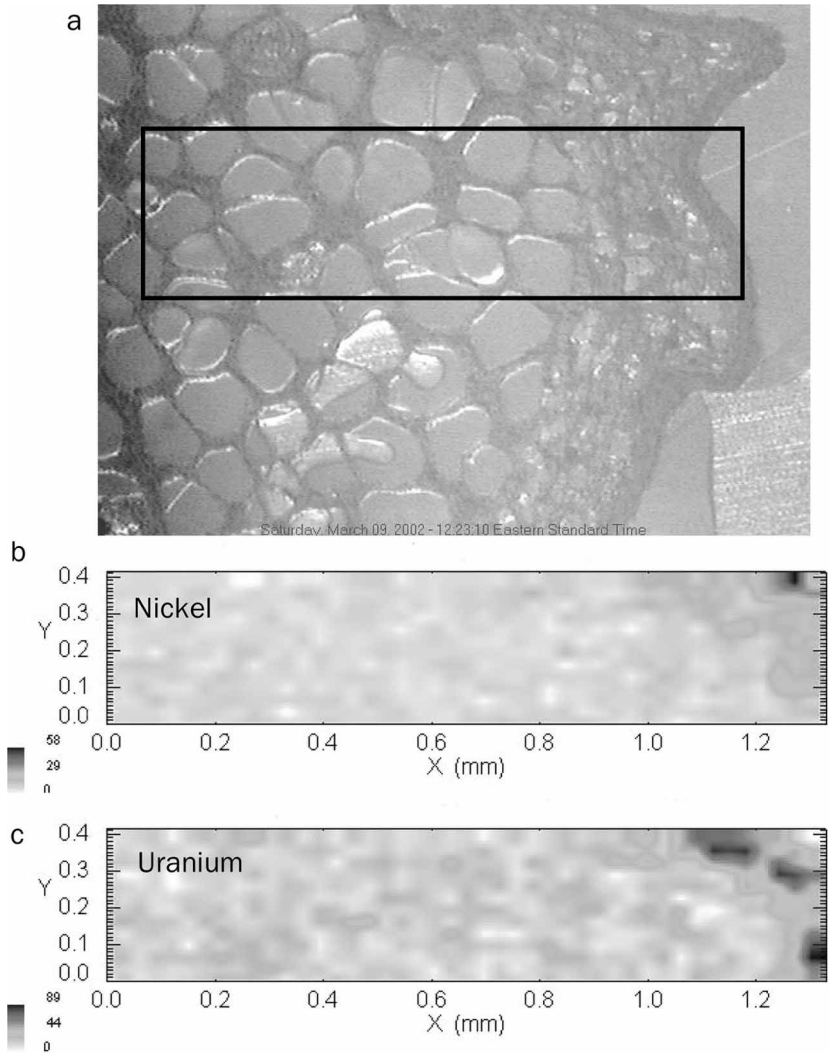

Figure 2. Photomicrograph image of (a) a lignified root collected from a U-enriched area of the Steed Pond former floodplain, showing the area from which XRF data was collected, (b) elemental map of Ni, and (c) U. Legends indicate raw fluorescence counts.

Uranium and Nickel in Micro-Rhizospheres

Figure 3 shows elemental maps of contaminants of concern collected from micro-rhizospheres 5 days and 32 days after wheat seedlings were killed. Care was taken to generate elemental maps of regions where the root tissue was clearly visible with the sample CCD camera. In 5-day-old samples, the root path is clearly visible in both the Ni and U maps, suggesting

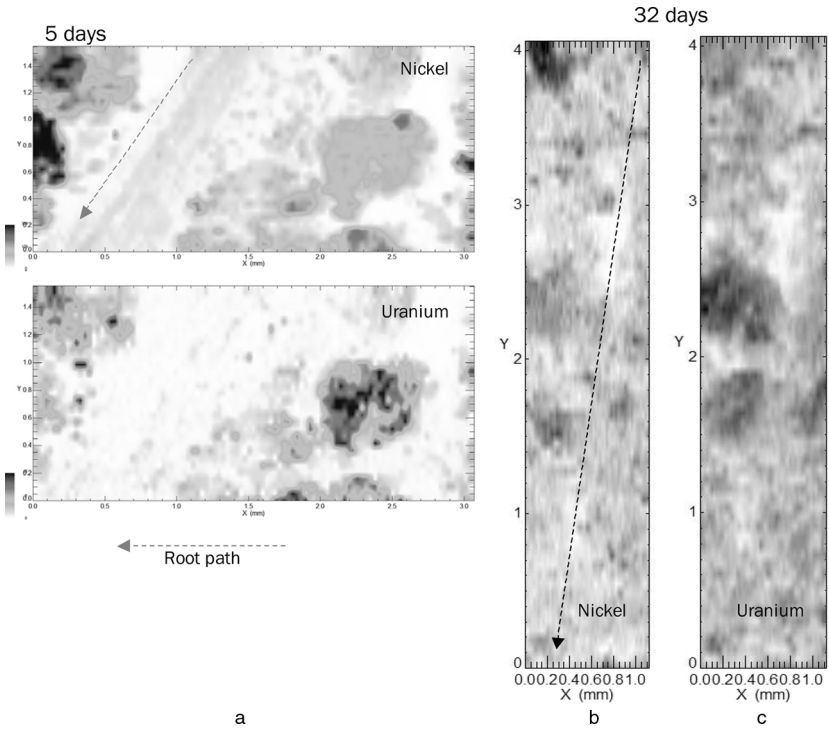

Figure 3. Micro-XRF image of cross sections of micro-rhizosphere consisting of wheat (*Triticum aestivum* L.) roots and contaminated soil collected from Lower Tims Branch after 5 days (1.5 mm × 3 mm) and 32 days (4 mm × 1 mm) of decomposition showing Ni and U.

concentrations are much lower inside the root tissue than in the soil. Low concentrations of Ni can be seen inside the root cross-section, whereas the exclusion of U from root tissue supports findings that U is not readily bioavailable in this system. After 32 days however, although the root is still visible using the sample CCD camera, its path through the soil particles can no longer be discerned from either the Ni or U maps. This apparent "disappearance" of the root from the elemental maps may be indicative of the loss of metabolic control over cation uptake at the cell wall, decomposition of cell membranes and loss of contents, as well as the increasing association of U with decaying organic material in the soil.

Study 2. X-Ray Fluorescence Computed Microtomography of Ni in the Vascular System of *Salix nigra* L.

μSXRF mapping of localized regions of significant Ni enrichment in *S. nigra* collected from Steed Pond (Fig. 4a) indicated that Ni was located entirely

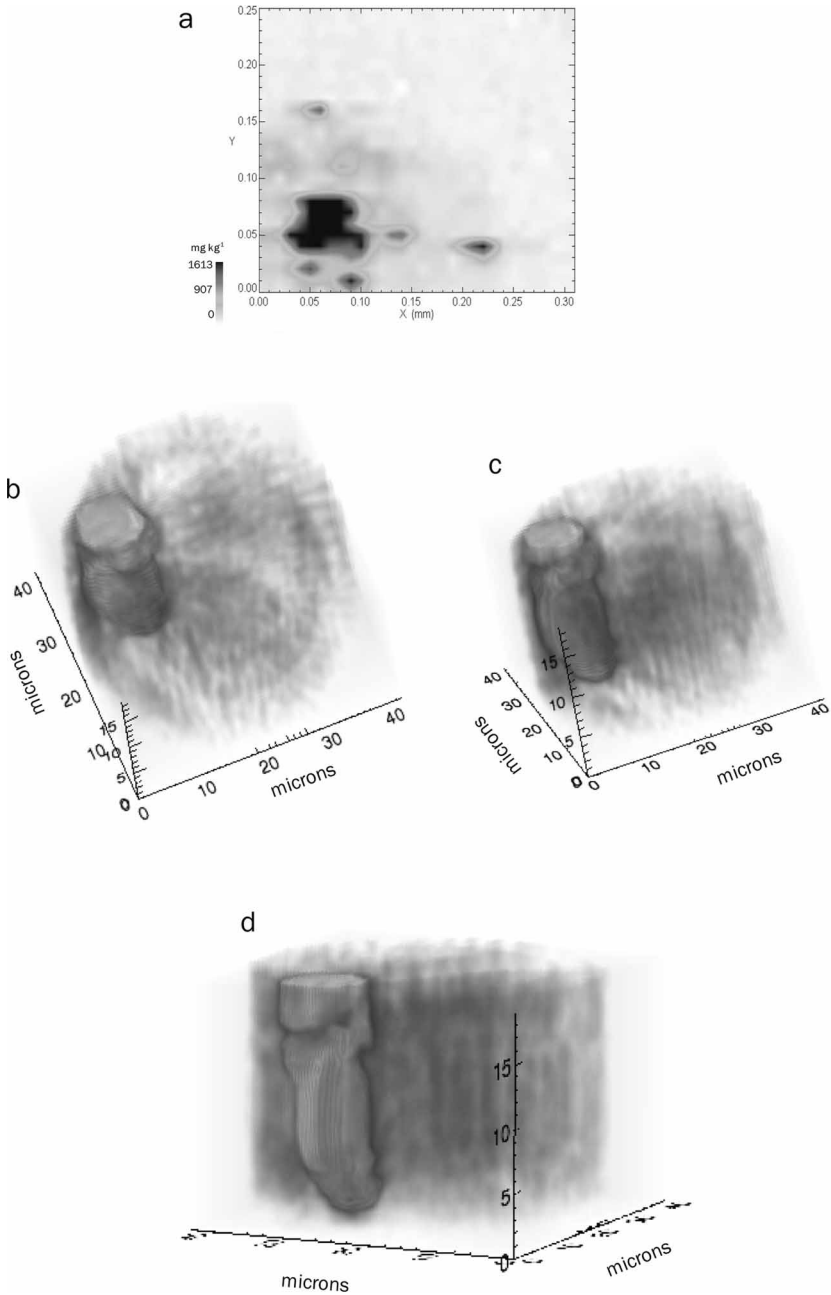

Figure 4. (a) Micro-XRF image (0.31 mm × 0.25 mm) of a Ni-enriched region within the woody tissue of *Salix nigra* L. collected from Steed Pond (from Punshon et al.[19], (b–d) three-dimensional tomographic reconstructions of Ni within the same sample.

within the lumen of a xylem vessel, and not within the cell walls.[19] Figures 4b–4d are three-dimensional tomographic reconstructions of Ni Kα fluorescence intensity in this same section of woody tissue excised from the core sample, with the aspect of observation ranging from above (Fig. 4b) to adjacent to the sample (Fig. 4d). The light gray areas are areas of low Ni Kα intensity in the matrix of the sample. The dark gray areas show the highest Ni intensity, clearly showing a cylindrical distribution of elevated Ni, consistent with the confinement of a Ni-enriched substance occupying the lumen of a xylem vessel.

Study 3. Selenium Distribution and Speciation in Mouthparts of Bullfrog Tadpoles (*Rana catesbeiana*)

Bullfrog larvae collected from the D-area ash basins exhibited oral abnormalities consistent with previous observations[42,52] (Figs. 5a and 5b). These

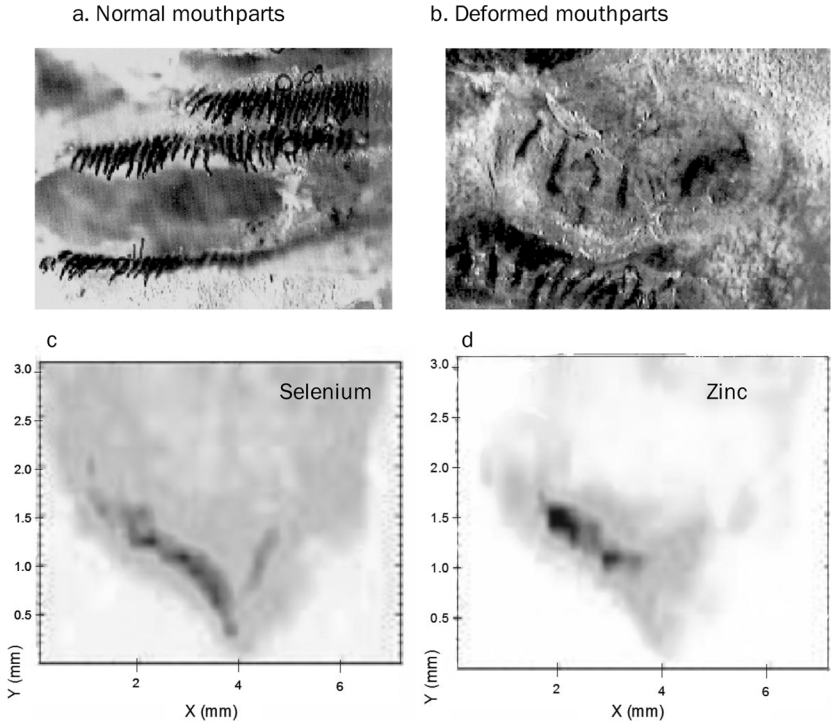

Figure 5. Photomicrograph of (a) normal and (b) abnormal mouthparts of bullfrog tadpoles *Rana catesbeiana*, and μSXRF images (6 mm × 3 mm) of (c) Se and (d) Zn distribution within abnormal mouthparts collected from the D-area ash basins.

abnormalities were seen as distorted and missing "toothrows" and distorted labial tissue. Initial μSXRF studies of the sectioned mouthparts indicated correlation between areas of increased Se and Zn concentrations (Figs. 5c and 5d). However, while Zn was more localized in the teeth region, and occurred in both control and exposed animals, Se was more evenly distributed throughout the soft tissue but occurred only in the animals collected from the ash basins. This would suggest that Zn is constituent of proteins that comprise the keratinized tooth rows.

Selenium in coal fly ash is relatively soluble and is exclusively inorganic in speciation with both selenite (Se IV) and selenate (Se VI) oxyanions having been identified in coal fly ash leachates.[53,54] However, Se is also known to be readily accumulated in biota, where it is predominantly found in an organic form, either as Se-amino acids, or as Se incorporated into proteins.[55] Indeed, the rapid accumulation of Se in the food chain has been identified as a potential environmental "time bomb" for fish.[56] In this study, we used μXANES to identify the Se oxidation state in the "hotspots" identified by μSXRF. The stable oxidation states of Se (VI, IV, 0 and −II) can be readily identified by XANES from position of the adsorption edge. Initial XANES analysis (Fig. 6) confirmed that Se in the sectioned mouthparts occurred in the reduced (− II) form consistent with its incorporation into organic molecules; the slightly higher edge position for the

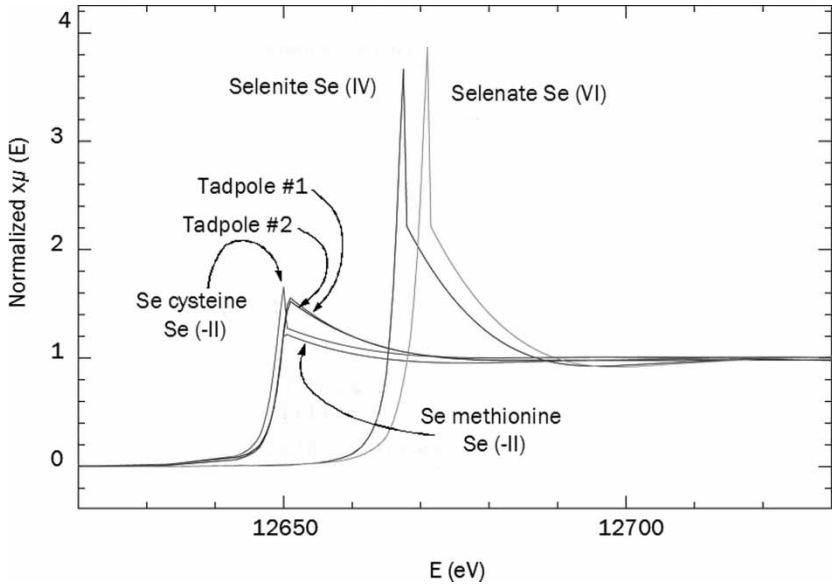

Figure 6. X-ray absorption near-edge spectroscopy spectra for Se inorganic and amino acid standards alongside spectra generated from bullfrog tadpole mouth sections.

samples may be due to surface binding of inorganic Se. The results confirm Se incorporation into the soft tissue of exposed organisms, and the oxidation state of Se (−II) is consistent with an organo-Se compound most likely from Se incorporation into proteins.

CONCLUSIONS

The application of μSXRF, CMT, and μXANES to biological tissue can provide robust qualitative data about the behavior and effect of metals and metalloids in exposed biota that would be impossible to achieve using conventional destructive volume-averaged techniques. Under ideal conditions, μSXRF can also be used to measure elemental abundance and can have detection limits in the sub $\mu g\, g^{-1}$ range.[47] Sensitivities in the range of $50-100\, ng\, g^{-1}$ have also been reported for many elements at third-generation facilities.[57–59] In general, biological samples are low atomic number (Z) matrices, which have less backscattering and lower spectral baselines, higher sensitivity, and significantly less self-absorption of x-rays by the sample. As a result, μSXRF is rapidly becoming a powerful research tool in biogeochemical research.

In the vascular tissues of trees, radial metal mobility or "post-growth translocation" between annual rings is thought to confound the use of tree rings as reliable biomonitors. Computer microtomography has generated an image of a Ni-rich substance confined within the xylem vessel of a willow, which shows no sign of radial transport. Therefore, in this situation at least, the use of willows as biomonitors of historical metal enrichment appears feasible. Imaging the Ni as it moves through an individual xylem vessels using CMT also illustrates that lower resolution measurements (i.e., larger beam area) of the metal distribution of annual rings is actually the sum of a large number of small vessel elements, whose metal content depends upon the presence or absence of metal moving through it, as well as on the probability that the sampling technique adequately captures the metal at the cut surface of the sample. The image of a discrete "slug" of metal adhering to the interior xylem vessel walls (and not to others in the immediate vicinity) reveals a level of stochasticity that future sampling techniques will have to take into account.

Finding accumulation of Se within deformed mouthparts of amphibians in the D-area ash basins suggests a direct cause-and-effect relationship between contaminants associated with coal combustion waste disposal and deleterious effects on biota. Spatially resolved elemental mapping of biota exposed to multiple contaminants, such as the ash basin, can potentially reveal the involvement of a particular element that would otherwise be masked in the traditional determination of body burdens. Although the involvement of other elevated metals or metalloids cannot be completely ruled out in this instance, it is clear that Se is highly concentrated in the

proteinaceous structures of the tadpole, such as the mouth, fins, and tail, to which a mode of action—indiscriminate substitution of Se into proteins—can be tentatively assigned.

There are, however, important experimental considerations to be made when analyzing biological tissues via μSXRF. The abilities of the researcher to interpret elemental maps generated by μSXRF is subject to error. These errors can arise from the effect of the escape depth (defined as distance from the sample surface from which fluorescence can be returned to the detector) combined with sample orientation. In biological samples, which are often sliced somewhat thicker than geological samples (several hundred micrometers in comparison with $\sim$30 μm), the generation of a two-dimensional map from a three-dimensional sample can cause gross misinterpretations about the anatomical structure of the sample. In this case, CMT is more informative than two-dimensional μSXRF images.

Interpreting elemental maps from biological tissue exposed to metals or metalloids requires comparison with tissues that have been collected from a pristine or reference uncontaminated area, as well as rigorous appropriate spatial statistical analysis. Frequently with synchrotron x-ray microanalysis, severe time constraints operate on the experimenter, and the production of replicated elemental maps of a metal-free control samples is prohibitive and replaced by volume-averaged data. Furthermore, it is becoming increasingly problematic to find pristine samples for some ubiquitous metal contaminants (for example, Pb) from ecosystems that are ecologically comparable. The application of statistical analyses to μSXRF maps is also a growth area within the field, and spatial statistical analyses that have been used for some time in geological mapping and landscape studies, such as cluster recognition analysis, are being applied to elemental maps.[60]

Synchrotron-based microprobe techniques are well suited to the study of biological tissues. Elemental mapping of flora and fauna from contaminated environments with μSXRF and CMT show localization of metals within distinct anatomical features, such as xylem vessels and mouthparts, which has allowed informed inferences to be made about mechanisms of transport and modes of action of contaminants that greatly benefit the study of bioavailability and trophic transfer.

ACKNOWLEDGMENTS

We gratefully acknowledge the technical assistance of Bill Rao of the National Synchrotron Light Source. This research was supported by Financial Assistance Award DEFG2600NT-40938 from the U.S. Department of Energy (DOE) to the Consortium for Risk Evaluation and Stakeholder Participation (CRESP). This research was partially supported by the Environmental Remediation Science Division of the Office of Biological

and Environmental Research, U.S. DOE through the financial assistance award no. DE-FC09-96SR18546 to the University of Georgia Research Foundation, EMSP grant 86845, and NIEHS (ESO 5022). Research carried out at NSLS, Brookhaven National Laboratory, is supported by the U.S. Department of Energy, Division of Materials Sciences and Division of Chemical Sciences, under contract DE-AC02-98CH10886. Use of the Beamline X26A was also partially supported by the Department of Energy, Basic Energy Science's Geosciences Research Program, under grant no. DE-FG02-92ER14244. Portions of this work were also performed at GeoSoilEnviroCARS (Sector 13), Advanced Photon Source (APS), Argonne National Laboratory. GeoSoilEnviroCARS is supported by the National Science Foundation–Earth Sciences (EAR-0217473), Department of Energy–Geosciences (DE-FG02-94ER14466), and the State of Illinois. Use of the APS was supported by the U.S. Department of Energy, Basic Energy Sciences, Office of Energy Research, under contract no. W-31-109-Eng-38.

REFERENCES

1. Bertsch, P. M.; Hunter, D. B. Application of synchrotron-based x-ray microprobes. *Chem. Rev.* **2001**, *101*, 1809–1842.
2. Koutzenogii, K. P.; Savchenko, T. I.; Chankina, O. V.; Kovalskaya, G. A.; Osipova, L. P.; Bgatov, A. V. Synchrotron radiation X-ray fluorescence analysis (SRXRF) for measuring the multielement composition of samples of biogenic nature. *J. Trace. Microprobe T.* **2003**, *21* (2), 311–325.
3. Pinheiro, T.; Alves, L. C.; Barreiros, A.; Araujo, F.; Bohic, S.; Simionovici, A. Imaging and quantification of trace metals in thin biological specimens using microprobe techniques: synchrotron induced X-ray fluorescence microprobe and nuclear microprobe. *Journal de Physique IV.* **2003**, *104*, 321–324.
4. Howe, J. A.; Loeppert, R. H.; Derose, V. J.; Hunter, D. B.; Bertsch, P. M. Localization and speciation of chromium in subterranean clover using XRF, XANES and EPR spectroscopy. *Environ. Sci. Technol.* **2003**, *37*, 4091–4097.
5. Arai, Y.; Lanzirotti, A.; Sutton, S.; Davis, J. A.; Sparks, D. L. Arsenic speciation and reactivity in poultry litter. *Environ. Sci. Technol.* **2003**, *37*, 4083–4090.
6. Ide-Ektessabi, A.; Fujisawa, S.; Sugimura, K.; Kitamura, Y.; Gotoh, A. Quantitative analysis of zinc in prostrate cancer tissues using synchrotron radiation microbeams. *X-Ray Spectrometry* **2002**, *31* (1), 7–11.
7. Ide-Ektessabi, A.; Kawakami, T.; Watt, F. Distribution and chemical state analysis of iron in the Parkinsonian substantia nigra using synchrotron radiation microbeams. *Nucl. Instrum. Methods Phys. Res. Section B: Beam Interactions with Materials and Atoms* **2003**, *213*, 590–594.
8. Szczerbowska-Boruchowska, M.; Lankosz, M.; Ostachowicz, J.; Adamek, D.; Krygowska-Wajs, A.; Tomik, B.; Szczudlik, A.; Simionovici, A.; Bohic, S. Topographic and quantitative microanalysis of human central nervous system tissue using synchrotron radiation. *X-Ray Spectrometry* **2004**, *33* (1), 3–11.
9. Salt, D. E.; Prince, R. C.; Pickering, I. J. Chemical speciation of accumulated metals in plants: evidence from X-ray absorption spectroscopy. *Microchem. J.* **2002**, *71* (2–3), 255–259.

10. Robinson, B. H.; Lombi, E.; Zhao, F. J.; McGrath, S. P. Uptake and distribution of nickel and other metals in the hyperaccumulator Berkheya coddii. *New Phytol.* **2003**, *158* (2), 279–285.
11. Küpper, H.; Lombi, E.; Zhao, F. J.; Wieshammer, G.; McGrath, S. P. Cellular compartmentation of nickel in the hyperaccumulators *A lyssum lesbiacum, Alyssum bertolonii* and *Thlaspi goesingense*. *J. Exp. Bot.* **2001**, *52* (365), 2291–2300.
12. Sarret, G.; Vangronsveld, J.; Manceau, A.; Musso, M.; D'Haen, J.; Menthonnex, J. J.; Hazemann, J. L. Accumulation forms of Zn and Pb in *Phaseolus vulgaris* in the presence and absence of EDTA. *Environ. Sci. Technol.* **2001**, *35* (13), 2854–2859.
13. de la Rosa, G.; Peralta-Videa, J. R.; Montes, M.; Parsons, J. G.; Cano-Aguilera, I.; Gardea-Torresdey, J. L. Cadmium uptake and translocation in tumbleweed (*Salsola kali*), a potential Cd-hyperaccumulator desert plant species: ICP/OES and XAS studies. *Chemosphere* **2004**, *55* (9), 1159–1168.
14. Sarret, G.; Saumitou-Laprade, P.; Bert, V.; Proux, O.; Hazemann, J. L.; Traverse, A. S.; Marcus, M. A.; Manceau, A. Forms of zinc accumulated in the hyperaccumulator Arabidopsis halleri. *Plant Physiol.* **2002**, *130* (4), 1815–1826.
15. Küpper, H.; Mijovilovich, A.; Meyer-Klaucke, W.; Kronek, M. H. Tissue- and age-dependant differences in the complexation of cadmium and zinc in the cadmium/zinc hyperaccumulator *Thlaspi caerulescens* (Ganges Ecotype) revealed by X-Ray Absorption Spectroscopy. *Plant Physiol.* **2004**, *134*, 748–757.
16. Naftel, S. J.; Martin, R. R.; Jones, K. W.; Feng, H.; Savard, M. M.; Begin, C. Synchrotron radiation analysis of a smelter impacted tree-ring sample. *Can. J. Anal. Sci. Spect.* **2001**, *46* (4), 118–122.
17. Martin, R. R.; Sham, T. K.; Wong Won, G.; Jones, K. W.; Feng, H. Synchrotron x-ray fluorescence and secondary ion mass spectrometry in tree ring microanalysis: applications to dendroanalysis. *X-Ray Spectrometry* **2001**, *30*, 338–341.
18. Martin, R. R.; Sham, T. K.; Won, G. W.; van der Heide, P.; Jones, K. W.; Song, S. R.; Protz, R. Secondary ion mass spectroscopy and synchrotron X-ray fluorescence in the study of the qualitative variation in metal content with time in tree rings. *Canadian Journal of Forest Research–Revue Canadienne De Recherche Forestiere* **1998**, *28* (10), 1464–1470.
19. Punshon, T.; Bertsch, P. M.; Lanzirotti, A.; McLeod, K. W.; Burger, J. Geochemical signature of contaminated sediment remobilization revealed by spatially resolved X-ray microanalysis of annual rings of *Salix nigra* L. *Environ. Sci. Technol.* **2003**, *37* (9), 1766–1774.
20. Siurek, J.; Chevallier, P.; Ro, C.; Chun, H. Y.; Youn, H. S.; Zieba, E.; Kuczumow, A. Studies on the wood tissue substitution by silica and calcite during the presevation of fossil wood. *J. Alloy Compd.* **2004**, *362* (1–2), 107–115.
21. Kuczumow, A.; Chevallier, P.; Dillmann, P.; Wajnberg, P.; Rudas, M. Investigation of petrified wood by synchrotron X-ray fluorescence and diffraction methods. *Spectrochim. Acta B* **2000**, *55* (10), 1623–1633.
22. Viksna, A.; Lindgren, E. S.; Standzenieks, P. Analysis of pine needles by XRF scanning techniques. *X-Ray Spectrometry* **2001**, *30* (4), 260–266.
23. de Jesus, E. F.O.; Simabuco, S. M.; dos Anjos, M. J.; R.T. L. Sychrotron radiation X-ray fluorescence analysis of trace elements in *Nerium oleander* for pollution monitoring. *Spectrochim. Acta B* **2000**, *55*, 1181–1187.
24. Varga, A.; Martinez, R. M. G.; Zaray, G.; Fodor, F. Investigation of effects of cadmium, lead, nickel and vanadium contamination on the uptake and transport

processes in cucumber plants by TXRF spectrometry. *Spectrochim. Acta B* **1999**, *54* (10), 1455–1462.
25. Sarret, G.; Schroeder, W. H.; Marcus, M. A.; Geoffroy, N.; Manceau, A. Localization and speciation of Zn in mycorrhized roots by mu SXRF and mu EXAFS. *Journal de Physique IV.* **2003**, *107*, 1193–1196.
26. Naftel, S. J.; Martin, R. R.; Sham, T. K.; Macfie, S. M.; Jones, K. W. Micro-synchrotron X-ray fluorescence of cadmium-challenged corn roots. *J. Electron Spectrosc. Relat. Phenom.* **2001**, *119* (2–3), 235–239.
27. Amblard-Gross, G.; Ferard, J. F.; Carrot, F.; Bonnin-Mosbah, M.; Maul, S.; Ducruet, J. M.; Coddeville, P.; Beguinel, P.; Ayrault, S. Biological fluxes conversion and SXRF experiment with a new active biomonitoring tool for atmospheric metals and trace element deposition. *Environ. Pollut.* **2002**, *120* (1), 47–58.
28. Panak, P. J.; Knopp, R.; Booth, C. H.; Nitsche, H. Spectroscopic studies on the interaction of U(VI) with Bacillus sphaericus. *Radiochimica Acta* **2002**, *90* (9–11), 779–783.
29. Twining, B. S.; Baines, S. B.; Fisher, N. S.; Jacobsen, C.; Maser, J. Quantification and localization of trace metals in natural plankton cells using a synchrotron x-ray fluorescence microprobe. *Journal de Physique IV.* **2003**, *104*, 435–438.
30. Hunter, D. B.; Bertsch, P. M.; Kemner, K. M.; Clark, S. B. Distribution and chemical speciation of metals and metalloids in biota collected from contaminated environments by spatially resolved XRF, XANES, and EXAFS. *Journal de Physique IV.* **1997**, *7* (C2), 767–771.
31. US-DOE. Linking Legacies: Connecting the Cold War Nuclear Weapons Production Processes to their Environmental Consequences; United States Department of Energy: Washington, DC, 1997 DOEEM-0319 232.
32. Pickett, J. B. *Heavy metal contamination in Tim's Branch sediments*; Westinghouse Savannah River Company: Aiken, SC, 1997 OPS-RMT-90-900200.
33. Khijniak, T. V.; Noval, M. T.; Sowder, A. G.; Bertsch, P. M.; Morris, P. J. Impact of nickel and uranium contamination on microorganisms in the Steed Pond corridor at the Savannah River Site. In *Proceedings of American Society for Microbiology 100th General Meeting*; Los Angeles, CA; American Society for Microbiology, Washington, DC, 2000.
34. Sowder, A. G.; Bertsch, P. M.; Morris, P. J. Partitioning and availability of uranium and nickel in contaminated riparian sediments. *J. Environ. Qual.* **2003**, *32*, 885–898.
35. Punshon, T.; Bertsch, P. M.; Lanzirotti, A.; Burger, J. Spatially resolved X-ray microanalysis of nickel in *Salix nigra* L. tree cores from an aged contaminated site. National Synchrotron Light Source–Brookhaven National Laboratory: Upton, NY, 2001; Annual Activity Report 2001: PUNS258, 2001. Available at: http://www.pubs.bnl.gov/nsls01/pdf/section%206%20abstracts/puns259.pdf.
36. Punshon, T.; Bertsch, P. M.; Lanzirotti, A.; Burger, J. Investigation of Spatial Heterogeneity in Ni Distribution Among Annual Rings of *Salix nigra* (black willow) Inhabiting a Former Radiological Settling Pond. National Synchrotron Light Source–Brookhaven National Laboratory: Upton, NY, 2002. Annual Activity Report 2002: PUNS0204, 2002.
37. Batson, V. L.; Bertsch, P. M.; Herbert, B. E. Transport of anthropogenic uranium from sediments to surface waters during episodic storm events. *J. Environ. Qual.* **1996**, *25*, 1129–1137.

38. Punshon, T.; Jackson, B. P.; Bertsch, P. M.; Burger, J. Mass loading of nickel and uranium on plant surfaces: Application of LA-ICP-MS. *J. Environ. Monit.* **2004**, *6* (2), 153–159.
39. Punshon, T.; Gaines, K. F.; Bertsch, P. M.; Burger, J. Bioavailability of uranium and nickel to vegetation in a contaminated riparian ecosystem. *Environ. Toxicol. Chem.* **2003**, *22* (5), 1146–1154.
40. Hopkins, W. A.; Mendonca, M. T.; Rowe, C. L.; Congdon, J. D. Elevated trace element concentrations in southern toads, *Bufo terrestris*, exposed to coal combustion waste. *Arch. Environ. Contam. Toxicol.* **1998**, *35*, 325–329.
41. Rowe, C. L.; Hopkins, W.; Congdon, J. D. Ecotoxicological implications of aquatic disposal of coal combustion residues in the United States: a review. *Environ. Monit. Assess.* **2002**, *80*, 207–276.
42. Rowe, C. L.; Kinney, O. M.; Fiori, A. P.; Congdon, J. D. Oral deformities in tadpoles (*Rana catesbeiana*) associated with coal ash deposition: Effects on grazing ability and growth. *Freshwater Biol.* **1996**, *36*, 723–730.
43. Jackson, B. P.; Allen, P. L.S.; Hopkins, W. A.; Bertsch, P. M. Trace element speciation in largemouth bass (*Micropterus salmoides*) from a fly ash settling basin by liquid chromatography-ICP-MS. *Anal. Bioanal. Chem.* **2002**, *374* (2), 203–211.
44. Hopkins, W. A.; Rowe, C. L.; Congdon, J. D. Elevated trace element concentrations and standard metabolic rate in banded water snakes (*Nerodia fasciata*) exposed to coal combustion wastes. *Environ. Toxicol. Chem.* **1999**, *18* (6), 1258–1263.
45. Hopkins, W. A.; Congdon, J. D.; Ray, J. K. Incidence and impact of axial malformation in bullfrog larvae (*Rana cetesbeiana*) developing in sites polluted by a coal burning power plant. *Environ. Toxicol. Chem.* **2000**, *19* (4), 862–868.
46. Eng, P. J.; Newville, M.; Rivers, M. L.; Sutton, S. R. In *X-ray Microfocusing: Applications and Technique*; McNulty, I., Ed.; International Society for Optical Engineering: Bellingham, WA, **1998**; *3449*, 145.
47. Sutton, S. R.; Bertsch, P. M.; Newville, M.; Rivers, M. L.; Lanzirotti, A.; Eng, P. J. In *Applications of Synchrotron Radiation in Low-Temperature Geochemistry and Environmental Science*; Fenter, P. A., et al, Eds.; Mineralogical Society of America, Washington, DC 2002; pp. 429–483.
48. Burau, R. G. Environmental chemistry of selenium. *Calif. Agric.* **1985**, 16–18.
49. Lemly, A. D. Selenium in aquatic organisms. In *Environmental Contaminants in Wildlife: Interpreting Tissue Concentration*; Beyer, W. N., Heinz, G. H., Redmon-Norwood, A. W., Eds.; Lewis Publishers: Boca Raton, FL, 1996; pp. 427–445.
50. Lemly, A. D. Environmental implications of excessive selenium: a review. *Biomed. Environ. Sci.* **1997**, *10*, 415–435.
51. Punshon, T.; Gaines, K. F.; Jenkins, R. A., Jr. Bioavailability and trophic transfer of sediment bound Ni and U in a southeastern wetland system. *Arch. Environ. Contam. Toxicol.* **2003**, *44* (1), 30–35.
52. Burger, J.; Snodgrass, J. W. Oral deformities in several species of frogs from the Savannah River Site, USA. *Environ. Toxicol. Chem.* **2000**, *19* (10), 2519–2524.
53. Niss, N. D.; Schabron, J. F.; Brown, T. H. Determination of selenium species in coal fly ash extracts. *Environ. Sci. Technol.* **1993**, *27* (5), 827–829.
54. Jackson, B. P.; Miller, W. P. Arsenic and selenium speciation in coal fly ash extracts by ion chromatography-inductively coupled plasma mass spectrometry. *J. Anal. Atom. Spectrom.* **1998**, *13* (10), 1107–1112.

55. Fan, T. W. M.; Teh, S. J.; Hinton, D. E.; Higashi, R. M. Selenium biotransformation into proteinaceous forms by foodweb organisms of selenium-laden drainage waters in California. *Aquatic Toxicol.* **2002**, *57*, 65–84.
56. Lemly, A. D. Selenium impacts on fish: an insidious time bomb. *Hum. Ecol. Risk Assess.* **1999**, *5* (6), 1139–1151.
57. Ellis, A. T.; Potts, P. J.; Holmes, M.; Oliver, G. J.; Streli, C.; Wobrauschek, P. Atomic spectrometry update—x-ray fluorescence spectrometry. *J. Anal. Atom. Spectrom.* **1997**, *12* (11), R461–R490.
58. Torok, S. B.; Labar, J.; Schmeling, M.; Van Grieken, R. E. X-ray spectrometry. *Anal. Chem.* **1998**, *70* (12), 495r–517r.
59. Vekemans, B.; Janssens, K.; Vincze, L.; Aerts, A.; Adams, F.; Hertogen, J. Automated segmentation of mu-XRF image sets. *X-Ray Spectrometry* **1997**, *26* (6), 333–346.
60. Vogt, S.; Maser, J.; Jacobsen, C. Data analysis for X-ray fluorescence imaging. *Journal de Physique IV*. **2003**, *104*, 617–622.